10

Application and optical characteristics of single-crystal paratellurite in acousto-optics of the 0.355–5 μm and terahertz ranges

© G.I. Kropotov[1], V.E. Rogalin[2], I.A. Kaplunov[3], A.A. Shakhmin[1], S.A. Tretiakov[3], A.S. Guk[2,4]

[1] Tydex LLC,
194292 St. Petersburg, Russia
[2] Institute of Electrophysics and Electric Power Engineering of the Russian Academy of Sciences,
191186 St. Petersburg, Russia
[3] Tver State University,
170100 Tver, Russia
[4] PJSC Krasnogorsky Zavod named after S. A. Zverev,
143402 Krasnogorsk, Moscow Region, Russia

e-mail: grigorykropotov@tydex.ru, kaplunov.ia@tversu.ru, v-rogalin@mail.ru

Received August 27, 2023
Revised August 27, 2023
Accepted February 20, 2024

The optical transmission of single-crystal paratellurite grown from raw materials of different purity procured from different manufacturers was examined in a wide spectral range. The studies were carried out for three crystallographic directions corresponding to crystallographic planes (001), (100), and (110). Reflectance spectra were obtained, and the influence of surface treatment on spectral features was analyzed. A slight difference in transmittance spectra was noted for raw materials differing in impurity content by 3 orders of magnitude. The feasibility of application of devices based on paratellurite in the UV and terahertz ranges was discussed.

Keywords: paratellurite, acousto-optics, reflectance spectrum, transmittance spectrum.

DOI: 10.61011/EOS.2024.04.58888.5519-24

Introduction

Instruments (acousto-optic (AO) devices included) utilizing the effect of diffraction of light on phase gratings created by elastic waves in a material due to modulation of the refraction index are used in various fields for controlling laser radiation or spectral analysis of images. Paratellurite is one of the materials that are used most often for construction of AO devices operating in a wide spectral range (near UV, visible, near IR). Single crystals of paratellurite (tetragonal modification α-TeO_2 of tellurium dioxide) have a number of unique physical properties. A fine blend of these properties has ensured paratellurite a leading position among AO materials [1–4]. TeO_2 features a wide transparency range (wavelength $\lambda = 0.35 - 5.5\,\mu$m) without noticeable absorption bands. Crystals are practically insoluble in water and have low hardness, which makes them easy to process (cut, grind, and polish). Being a member of the tetragonal crystal system (point symmetry group 422), paratellurite exhibits a fairly strong birefringence (up to $+0.19$ in the visible range), which makes it suitable for application in acousto-optic electronically tunable filters and acousto-optic dispersive delay lines (AODLs). High refraction indices ($2.29 - 2.45$ at $\lambda = 0.5461\,\mu$m) of ordinary and extraordinary rays in combination with uniquely low—for solid materials—propagation velocities of ultrasound in the [110] direction (616 m/s) ensure that paratellurite has an unusually high value of AO quality factor $M_2 = n^6 p^2/\rho C_s^3$ (n is the refraction index, p is the effective photoelastic constant, ρ is the density, and C_s is the sound propagation velocity) [1–4].

Since AO device efficiency η ($\eta = I_d/I_0$, where I_0 is the incident light intensity and I_d is the intensity of diffracted light) depends proportionally on the value of M_2 and on the ultrasound power, the high M_2 value (in the most in-demand transparency range) of paratellurite determines its main technical advantage over other AO materials [5,6]. It consists in the potential for efficient control over light fluxes at low acoustic powers. The process is controlled by a signal from a high-frequency generator ($\sim 50 - 250$ MHz) with a power of $0.5 - 5$ W fed to a piezoelectric transducer [7–9]. Low power consumption makes forced cooling of an AO device unnecessary and provides comparatively low optical and acoustic distortions caused by heat release in the light-and-sound guide (LSG) [10–13].

These advantages have enabled the widespread use of paratellurite, which has found application in various devices. Elements for modulators controlling the intensity of electromagnetic radiation passing through the LSG are made from TeO_2. They allow one to transmit signals (information) via a laser beam. Modulators are also used for pulsed radiation output from laser cavities [2–5,14]. Paratellurite-based deflectors (scanners) utilize Bragg diffraction to control the direction of propagation of the output laser beam within a solid angle on the order of $3^\circ \times 3^\circ$ [4–6].

Acousto-optic deflectors (AODs) are used in laser locators, range finders, and engraving machines. The application

of AODs for controlling laser radiation with an operation speed of $20 - 50$ kHz is worth highlighting.

When using AODs, one needs to take into account a number of their specific features, such as a relatively small scanning angle (in most cases, no greater than $3^\circ \times 3^\circ$), the requirement for linear polarization of laser radiation, loss of controlled laser radiation (on the order of 20% when a two-coordinate deflector is used), and temperature dependence. The lack of moving elements, low energy consumption, simple design, and a microsecond response time are the unquestionable advantages of AODs.

Electronically tunable acousto-optic filters (AOFs) are used for the analysis of various kinds of optical data and spectral analysis of radiation (both passing through the medium under study and emitted by sources, such as stars, planets, flame plumes, etc.) [4,5,14]. Paratellurite is used in AOFs not only throughout the entire visible range, but also in the IR range (up to around $2 - 3\,\mu$m).

Adaptive AODLs constitute a novel class of AO devices that differ from traditional ones in having exceptionally broad spectra of electromagnetic and acoustic fields. A specific feature of AODLs is their unusually high spectral resolution, which should reach 10000 [15–17]. This is currently a record-high spectral resolution for AO devices (including those using femtosecond lasers in the near IR range, $0.8 - 1.5\,\mu$m).

AO processors are devices designed for spectral analysis of weak radio signals with background interference. This challenge is addressed by AO processors based on paratellurite crystals [18–20] that use the Fourier method to retrieve the spectrum of radio signals.

In classical optics, paratellurite is used (due to its exceptional birefringence in the visible and near IR ranges) to construct relatively large optical prisms. Paratellurite also has certain application prospects as a novel phase-shifting and magneto-optic material [21]. Unique piezoelectric properties could allow for the construction of new gyroscopic sensors and high-precision actuators of torsional microelectromechanical systems (MEMS) [22]. In nuclear physics, paratellurite is used to detect double beta decay events [23–26].

Progress in laser physics has led to the construction of industrial solid-state lasers operating at the third harmonic of fundamental radiation at 1064 nm (namely, at $\lambda = 355$ nm). These lasers are high-power and compact devices, thus having a wide application potential [27]. At present, collinear AO quartz cells are used in the UV range; the use of rare-earth tungstate crystals is promising, although the construction of AO two-coordinate deflectors based on paratellurite appears to be relevant for $\lambda = 355$ nm.

Potential applications of paratellurite in the terahertz (THz) wavelength range, where a shortage of natural optical materials is still being felt, have recently been investigated [28–32]. Specifically, the generation of THz radiation in α-TeO_2 single crystals irradiated with femtosecond laser pulses with a wavelength of 800 nm was reported in [29]. Paratellurite has relatively high absorption coefficient values ($\sim 10\,\text{cm}^{-1}$ at $\lambda = 300\,\mu$m and $\sim 2\,\text{cm}^{-1}$ at $\lambda = 800\,\mu$m) and a significant refraction index (~ 5.2) in the THz range [23,31]. Nevertheless, the high AO quality and high energy efficiency of AO devices [32] allow one to argue that TeO_2 has great potential in the design of AO modulators, deflectors, and filters of the far THz range. However, the optical properties of paratellurite in the THz region remain understudied. The values reported in literature [29,30] were determined in calculations based on a phenomenological model for materials with characteristic resonant frequencies (or other characteristic energy scales) for optical absorption (e.g., ionic and molecular vibrations and the Lorentz oscillator model).

The density of structural defects in crystals (impurities, dislocations) needs to be minimized for paratellurite to be used in acousto-optics. This is one of the primary goals of researchers working on the issues of growth of this material. Certain defects, such as gas bubbles, are totally unacceptable in an LSG material (at least in the volumes through which light and ultrasound are transmitted). Optical anomalies (OAs) in crystals, distortions of acoustic fronts, and enhanced attenuation of ultrasound are all associated with structural defects and mechanical stresses caused by them [33].

Despite the considerable progress achieved over the last 15–20 years in the field of growth of relatively large and optically homogeneous paratellurite single crystals, the issues of their further enlargement and reduction of impurity densities and optical losses associated with scattering and absorption of light still remain relevant today [34–44]. If paratellurite crystals have equally high structural and optical quality characteristics, their size becomes the decisive factor in choosing a material for certain applications (e.g., as an AODL light-and-sound guide). Since both the spectral resolution of filters and the delay time for a delay line, which also belongs to the class of AO filters, are directly proportional to the length of a light-and-sound guide, a need arises for large-diameter paratellurite that allows one to cut out an LSG up to $80 - 100$ mm in length along the direction of propagation of the laser beam [5].

Owing to the photoelastic effect, structural defects become the main cause of various optical inhomogeneities and anomalies in crystals, inducing an enhancement of absorption and scattering of radiation. In actual experiments, optical surfaces of crystal elements are never flat, since they have their own micro- and nano-relief that produces the diffuse component of reflection of light fluxes.

It should be noted that both absorption and scattering of light are also present in an ideal crystal. Absorption is caused by the interaction of electromagnetic waves with electron shells of atoms, while scattering is attributable to fluctuations of the refraction index and vanishes only at absolute zero (0 K). Therefore, improving the structural quality of crystals by optimizing growth technologies, one just gets closer to certain ideal values of optical parameters. Since the structural quality of real single crystals is very far

from ideal, any significant progress in growth technology is accompanied by an enhancement of optical characteristics.

The study of optical characteristics of paratellurite was initiated in [45,46]. Transmission spectra measured in crystal samples perpendicular and parallel to the optical axis were presented [45], and the dispersion for ordinary and extraordinary refraction indices from the UV transmission cutoff to $1\,\mu$m, the absorption coefficient in the visible region, and optical rotation were examined [46,47]. The authors of [48] have recorded reflection spectra in polarized light perpendicular and parallel to the optical axis at temperatures of 295 and 85 K within the $50-1000\,\mathrm{cm}^{-1}$ frequency spectral interval. The intensity distributions of scattered laser radiation at wavelengths of 488, 531, and 633 nm along the optical axis of paratellurite were visualized in [21]; the magnitudes of specific rotation were also calculated, and the optical rotation curve for the visible range was obtained.

According to the data from [40,41], the overall extinction coefficient, which includes the absorption and scattering coefficient at $\lambda = 0.535\,\mu$m, does not exceed $0.03\,\mathrm{cm}^{-1}$. In the near IR range, the extinction coefficient lies within the $(10^{-3}-10^{-2})\,\mathrm{cm}^{-1}$ interval. Fresnel reflection is minimized successfully by anti-reflective coatings. All of this combined provides an opportunity to construct paratellurite-based AO devices up to 60 mm (or more) in length and use fairly high-power continuous and pulsed lasers.

Spectra of the refraction index and the absorption coefficient were measured in [30] within the $0.25-2\,\mathrm{THz}$ $(1200-150\,\mu\mathrm{m})$ frequency range at room temperature by THz spectroscopy of a pure crystal of α-TeO_2 as a candidate material for THz applications. The measured absorption coefficients varied within the $1-100\,\mathrm{cm}^{-1}$ interval in the indicated spectra range. The absorption coefficient values were greater in the direction of light propagation corresponding to the extraordinary refraction index.

The authors of [49] have studied the electrodynamic characteristics of paratellurite within a wide frequency range at temperatures from 77 to 300 K using pulsed broadband THz spectroscopy and IR Fourier spectroscopy. Temperature evolution of the complex refraction index and the absorption of radiation along crystallographic directions [001] and [110] were estimated. It was found that the processes of intrinsic absorption are suppressed significantly at temperatures lower than 100 K. Temperature dependences of the refraction index and the absorption coefficient of paratellurite in the THz range were obtained. It was demonstrated that cooling of the crystal leads to a shift of the high-frequency THz absorption boundary from 15 to $40\,\mathrm{cm}^{-1}$ (from 670 to $250\,\mu$m, respectively) in the [001] crystallographic direction.

In the present study, the optical characteristics (transmittance and reflectance) of paratellurite grown from raw materials of different purity procured from different manufacturers were examined in a wide spectral range (UV–visible–IR–THz). Modern instruments forming a single measuring complex were used in these experiments. Samples representing the three main crystallographic directions for paratellurite ([110], [100], and [001]) were prepared. The characteristics of surfaces corresponding to the indicated crystallographic orientations were studied in detail.

Paratellurite samples for experiments

Samples provided by different manufacturers of single crystals grown from raw materials of varying degrees of purity were prepared for studies of the spectral characteristics of optical transmission of paratellurite. All the examined α-TeO_2 single crystals were grown by the Czochralski method in air under normal pressure.

At the Tver State University (TSU, https://tversu.ru/) and the „Elent A“ enterprise (Dnipro, www.elent-a.net), single crystals were grown in the [110] crystallographic direction, and their diameter was $60-80$ mm. The average dislocation density in single crystals was $(1.5-3.5)\cdot10^4\,\mathrm{cm}^{-2}$. TSU samples were prepared from single crystals grown from high-purity (the mass percentage of impurities was below 0.0001%) and chemically clean (99.5% purity) raw materials. „Elent A“ samples were grown from raw materials with the main substance being no less than 99.9995% pure. The results of atomic emission spectral analysis revealed that Fe, Cu, Al, Bi, and Mg were the main impurities in all samples.

Samples of three crystallographic directions ([110], [100], and [001]) were prepared for each type of crystals procured from different manufacturers and grown from materials of different purity.

Preparation of optical surfaces of paratellurite samples for transmittance and reflectance measurements

Samples were cut and ground by conventional techniques [50]. Fine grinding with a suspension of M10 (F800) grinding powder before polishing is considered to be sufficient for such a material as paratellurite. The size of the layer removed by grinding was monitored with an accuracy of $0.5\,\mu$m. The surface prepared for polishing was assessed visually using an $8^\times$ lens.

Differences between the three selected planes became apparent already at the stage of fine grinding with M10 powder. It was sufficient for plane (001) to remove a layer of material $10\,\mu$m in thickness. The surface „dullness“ and defects from the earlier M28 (F400) grinding disappear in the process. A 10-μm-thick layer is insufficient for plane (110); we had to remove $15-20\,\mu$m. The thickest layer (about $70\,\mu$m) was removed on the (100) plane. However, the durations of the process of fine grinding of each plane were the same; thus, the material removal rates differed several-fold. This is caused by differences in mechanical characteristics of the surface attributable to differences in

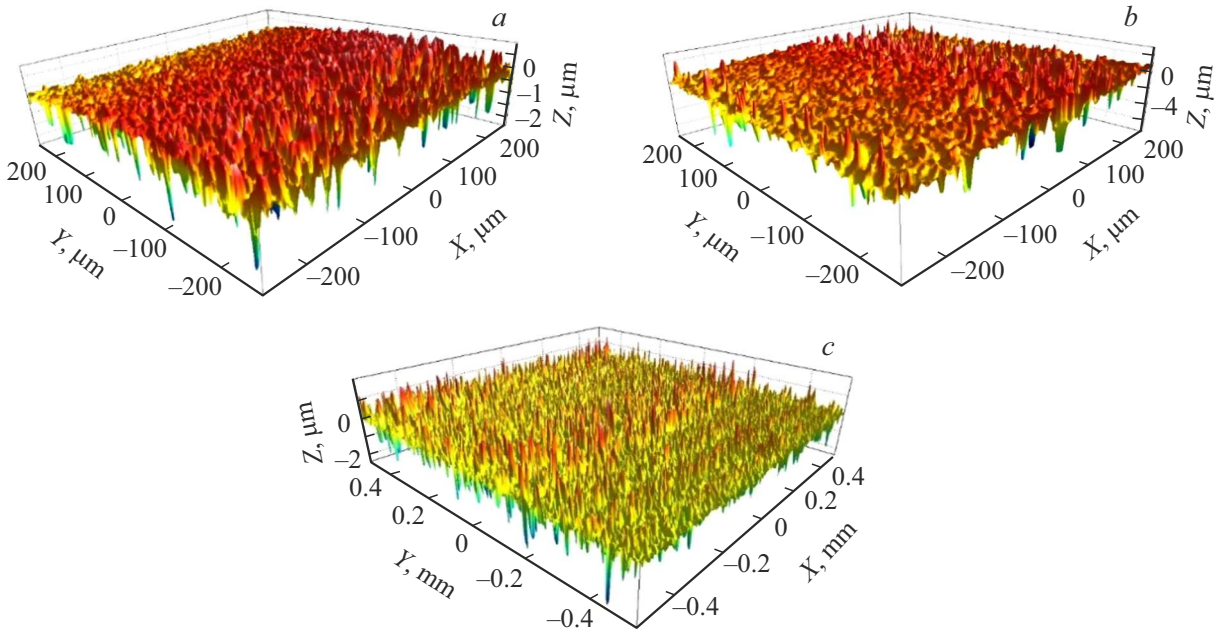

Figure 1. 3D surface profile of planes (001) (*a*), (100) (*b*), and (110) (*c*) after fine grinding with M10 powder.

Table 1. Surface characteristics of paratellurite samples after grinding

Parameter \ Plane	(001)	(100)	(110)
Average roughness of the 3D profile (Sa)	289.6 nm	594.6 nm	219.1 nm
Maximum height of the 3D profile (Sz)	3062.1 nm	10905.0 nm	4509.2 nm
Average roughness of the linear profile (Ra)	308.8 nm	488.5 nm	158.1 nm
Maximum roughness height of the linear profile (Rt)	2009.2 nm	3587.5 nm	1049.1 nm
Average maximum height of the linear profile (Rz)	1708.0 nm	2824.2 nm	928.4 nm
Average distance between irregularities of the 3D profile (Sm)	19.619 μm	22.097 μm	17.441 μm

reticular density of planes and orientation of Te–O bonds relative to the treated surface.

A NanoMap WLI1000 optical profilometer was used to examine the relief layer remaining after fine grinding and assess the dimensions of the cracked layer and the time needed to remove it by polishing. Figure 1 shows the surface profiles, and the average roughness parameters of the obtained surfaces are presented in Table 1.

On-machine polishing of surfaces was performed manually under a pressure of $0.7 - 0.8$ at using the standard method. The processing time was 1 h. A weakly alkaline polishing suspension with a pH of 10 was prepared from AM 0.5/0 diamond micropowder and distilled water with a modifying addition of NaOH. The use of alkali facilitates reaction

$$TeO_2 + 2NaOH = Na_2TeO_3 + H_2O$$

and „soft“ non-abrasive removal of a part of the surface layer material.

The thickness of the removed layer of sample material was monitored every 15 min of polishing using a thickness gauge with an accuracy of 0.5 μm; in addition, the surface was inspected visually. The thickness of material layers polished out in 1 h differed from one examined crystallographic plane to the other: 12 μm were removed from the (001) plane, and only 8 μm were removed from planes (110) and (100).

The samples prepared for measurements had the following characteristics of polished surfaces: flatness $N < 0.3$, $\Delta N < 0.1$; wedge angle $\Theta \sim 20''$; finish P = III. The end thickness of processed plates was 5.21 ± 0.01 mm.

Polished surfaces were examined using a NanoMap WLI1000 optical profilometer and the SPIP package; the surface roughness parameters were calculated using the specialized Gwyddion software.

Figures 2 and 3 present 3D and 2D surface profiles, and Table 2 lists the average surface characteristics of

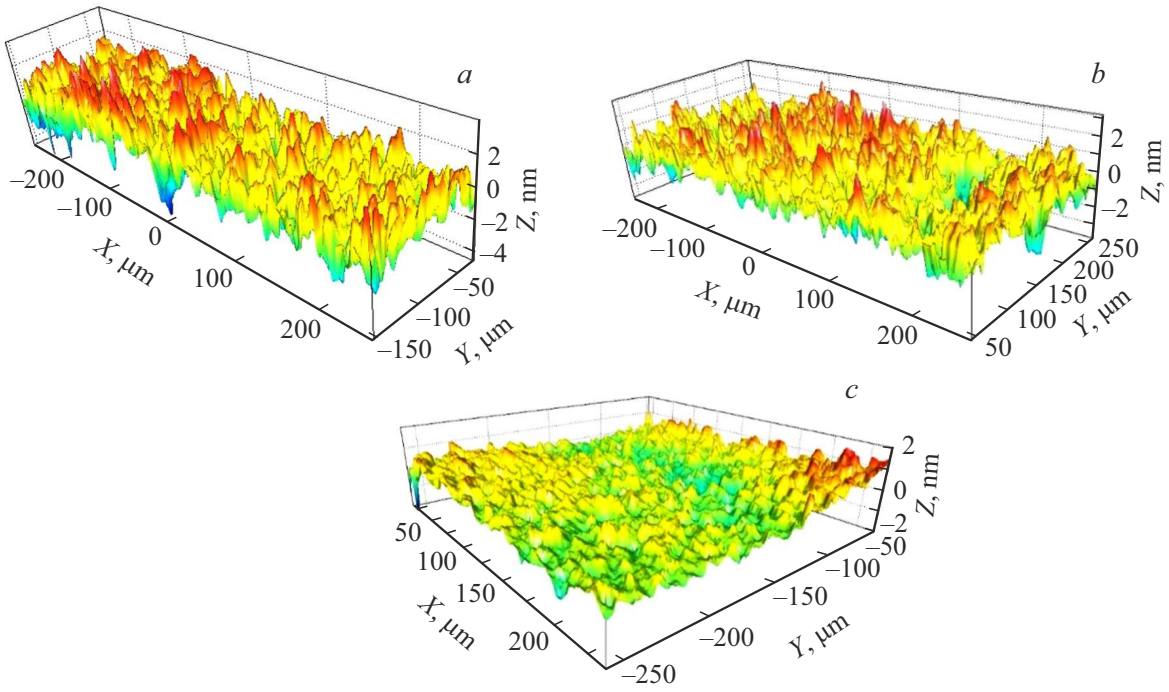

Figure 2. 3D profiles of surfaces (001) (*a*), (100) (*b*), and (110) (*c*) after polishing.

polished samples. It follows from the comparison with ground surfaces (Table 1) that the surface roughness and the height of irregularities decreased by 3 orders of magnitude. The distance between irregularities remained virtually unchanged.

The obtained measurement results suggest that the values of roughness parameters for different crystallographic planes subjected to polishing under the same conditions may differ by a factor of 2–3; this, in turn, may affect the values of reflection and transmission coefficients.

The difference in roughness parameter values corresponding to the studied crystallographic planes is attributable to a difference in surface energy. An analysis of geometry of polished crystallographic planes of paratellurite revealed that the minimum roughness and the minimum height of irregularities are found in the (110) plane. It is a singular face of a paratellurite crystal and the most closely packed plane with the minimum surface energy. It is in this direction that single crystals are grown from melt by the Czochralski method and the surface of the crystallization front, which, in an ideal scenario, matches the (110) plane in geometry, is formed. This allows one to obtain single crystals with a more perfect structure and a minimum concentration of gas inclusions.

To study the reflection from polished surfaces, three wedge-shaped samples were prepared with surface plane indices corresponding to the direction of samples examined for optical transmission: [110], [100], and [001]. The characteristics of the polished surface corresponded to those of treated surfaces discussed above; the remaining sample surfaces were matted. The angle between the surfaces of wedge-shaped samples ensured the lack of reflections from the second matte surface.

Equipment and procedures

The spectral transmittance of samples was measured using a Photon RT spectrophotometer (Essent Optics) and a Vertex 70 Fourier spectrometer (Bruker) within the $0.185 - 670\,\mu$m range. The spectral resolution of Photon RT within the $0.185 - 1.7\,\mu$m range was ~ 1 nm, and the measurement accuracy was as high as 0.01%. The accuracy of determination of the wave number with Vertex 70 was $0.3 - 0.5\,\text{cm}^{-1}$, and the photometric accuracy was 0.1%. Measurements within the $150 - 3000\,\mu$m range were carried out using a TeraK8 (MenloSystems) spectrometer; the spectral resolution was 1 GHz, and the error of transmittance measurements was $\sim 0.5\%$.

Transmittance measurements were performed in unpolarized light at wavelengths up to $300\,\mu$m (Photon RT spectrophotometer and Bruker Vertex 70 Fourier spectrometer). At wavelengths greater than $300\,\mu$m (TeraK8 MenloSystems spectrometer), radiation was polarized.

In order to eliminate measurement errors associated with the possible influence of the degree of polarization on the transmittance value, test studies of transmittance were conducted with a Photon RT spectrophotometer and polarized (s-polarization) radiation. It was found that light polarization has no effect on the transmittance of crystals.

Absorption (attenuation) coefficients α were calculated using the standard method with account for multiple reflections [51,52]. The values of reflection coefficients

Table 2. Surface characteristics of paratellurite samples after polishing

Parameter \ Plane	(001)	(100)	(110)
Average roughness of the 3D profile (Sa)	0.8 nm	0.7 nm	0.4 nm
Maximum height of the 3D profile (Sz)	7.8 nm	7.3 nm	4.0 nm
Average roughness of the linear profile (Ra)	0.7 nm	0.3 nm	0.2 nm
Maximum roughness height of the linear profile (Rt)	4.5 nm	2.0 nm	1.7 nm
Average maximum height of the linear profile (Rz)	3.7 nm	1.8 nm	1.4 nm
Average distance between irregularities of the 3D profile (Sm)	16.561 μm	17.980 μm	15.403 μm

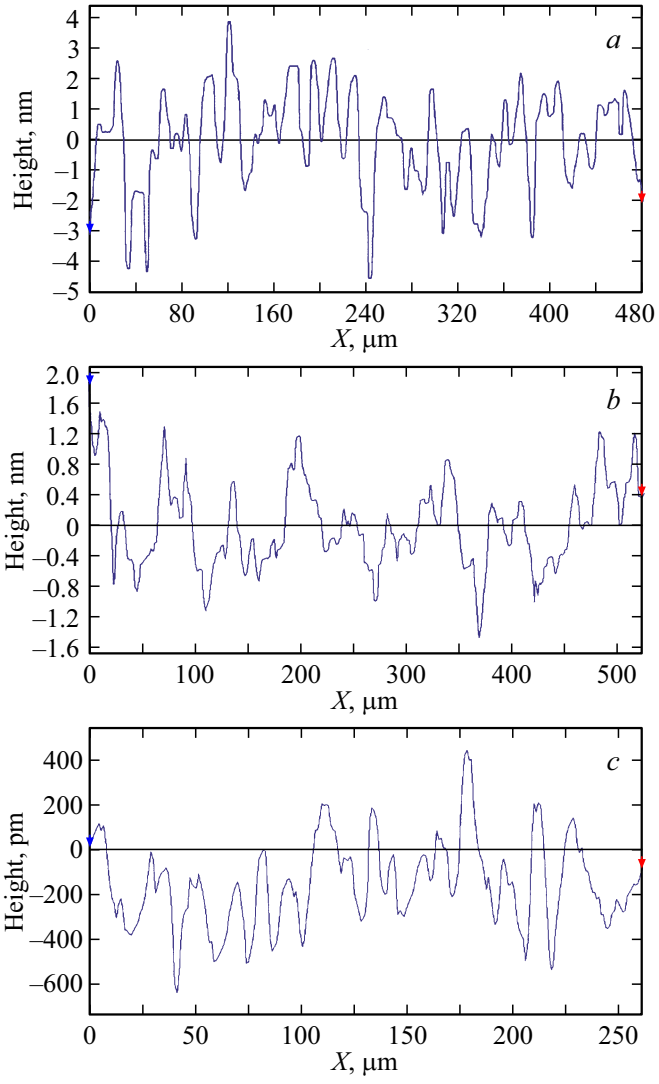

Figure 3. 2D profiles of surfaces (001) (*a*), (100) (*b*), and (110) (*c*) after polishing.

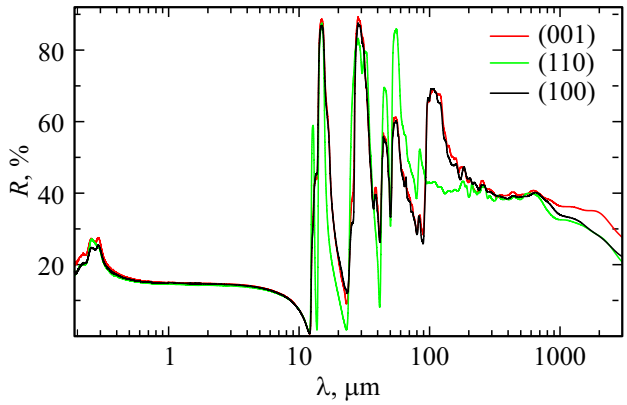

Figure 4. Reflectance spectrum in the UV, visible, IR, and THz ranges of wedge-shaped paratellurite samples of different crystallographic orientations.

for the studied crystals were determined throughout the entire examined range of wavelengths (a comparison was made with the data from [1,53] in the visible and near IR ranges). Absolute error of calculations $\Delta\alpha$ was determined in accordance with the procedure detailed in [54].

Results and discussion

Figure 4 shows the reflectance spectra recorded for wedge-shaped samples with surfaces corresponding to crystallographic planes (001), (100), and (110) in the UV, visible, IR, and THz spectral ranges.

In the visible range, reflectance increases with decreasing wavelength, and refraction index n in this wavelength range is $\sim 2.3-2.5$. The reflectance in the UV range peaks at 0.275 μm. The wavelength of 0.355 μm, which is the third harmonic of an Nd:YAG laser, corresponds to a reflectance of 19.2% (for radiation incident along the optical axis), and the corresponding value of n is 2.56.

The reflectance in the THz range is significantly higher. The refraction index of paratellurite determined based on reflectance dependencies in the THz range decreases with increasing wavelength and reaches a level of $\sim 4.4-5.1$ within the $130-700$ μm range. Its value ensures AO quality (M_2, for a transverse acoustic wave propagating along axis [110]). This is several orders of magnitude

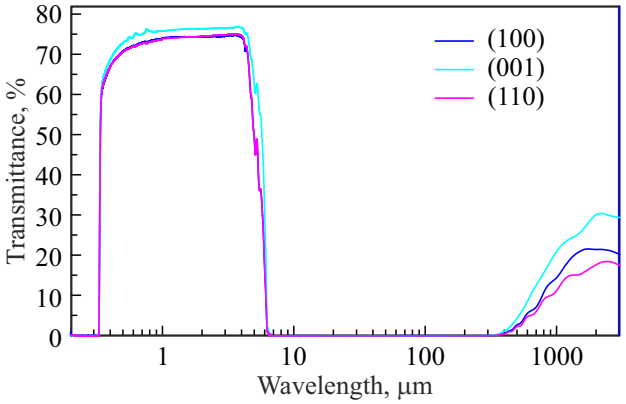

Figure 5. Transmittance spectrum of paratellurite, which was obtained from high-purity raw materials, with different crystallographic orientations.

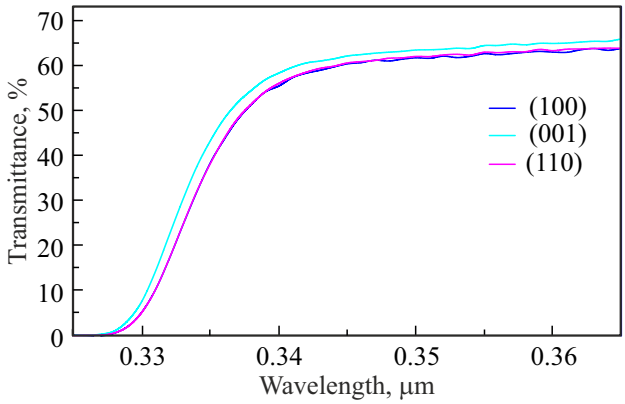

Figure 6. Spectral dependence of transmittance near the short-wave transmission cutoff of paratellurite of different crystallographic orientations obtained from high-purity raw materials.

higher than what is typical of most known materials in this range [32]. The value of n starts decreasing after $700\,\mu$m, dropping to ~ 2.6 at $3000\,\mu$m.

A series of minima and maxima with magnitudes ranging from 5 to 85% is seen in the reflectance spectrum within the $10-100\,\mu$m range. These features may be associated with an anomaly of refraction index dispersion; a similar pattern is observed in oxides (specifically, in SiO_2) and crystalline quartz. The peaks correspond to wavelengths approximately equal to 15, 30, 45, and $55\,\mu$m, which are multiples of the horizontal distance between surface irregularities (parameter Sm in Table 2; Fig. 3). This suggests the possible presence of a wave interference effect induced by material processing. Several studies focused on this feature of the paratellurite reflectance spectrum have already been published [29,30,48]. The reflection coefficient of paratellurite was measured in [48] within the range from 0 to $100\,\mathrm{cm}^{-1}$, and reflectance spectra with similar maxima and minima were obtained. We failed to determine the reasons for emergence of these peaks and troughs. Their emergence is thought to be associated with certain factors of experimental design or the presence of multiphonon processes. The same reflectance pattern was observed in [29] within the range up to 14 THz.

Figure 5 illustrates the influence of crystallographic orientation on the $0.185-3000\,\mu$m transmittance spectrum of paratellurite obtained from high-purity raw materials. The difference in transmittance of samples in the visible and IR ranges is $2-3\%$, within the $800-3000\,\mu$m range, this difference is significantly more profound and reaches $6-12\%$. The transmittance starts increasing significantly in the THz range at $\sim 340\,\mu$m and reaches its maximum around $1800-2100\,\mu$m. Single crystals with a crystallographic orientation corresponding to the (001) plane have the highest transmittance in the UV, visible, and THz ranges.

The short-wave transmission cutoff is characterized by its steep growth. The transmittance at $\lambda = 355\,$nm is as high as 64% (Fig. 6). The calculated spectra of attenuation

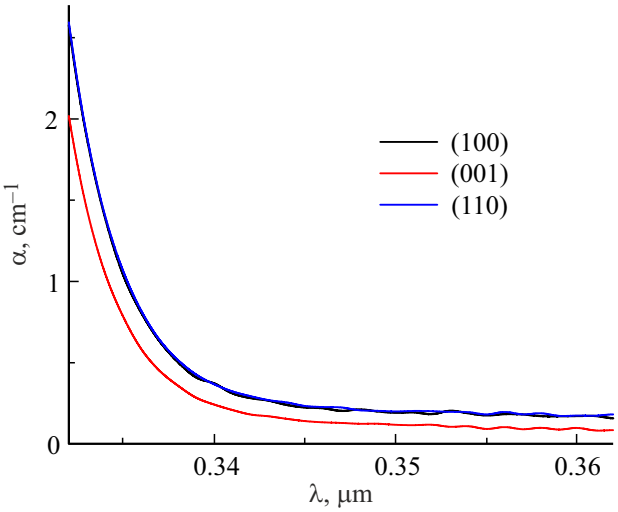

Figure 7. Short-wave region of the absorption spectrum of paratellurite of different crystallographic orientations obtained from high-purity raw materials.

(absorption) coefficients for the short-wave transmission cutoff and THz ranges are presented in Figs. 7 and 8, respectively. The absorption coefficient in the UV region at $\lambda = 0.355\,\mu$m is $0.092\,\mathrm{cm}^{-1}$. This value indicates a sufficiently high absorption, which precludes the use of paratellurite to control high-power continuous laser radiation; however, the material is suitable for application in low- and medium-power single-pulse sources.

In the THz spectral range, the absorption coefficient decreases from $20\,\mathrm{cm}^{-1}$ at $235\,\mu$m to $11\,\mathrm{cm}^{-1}$ at $300\,\mu$m; at $800\,\mu$m, the absorption coefficient is $1.7\,\mathrm{cm}^{-1}$; its minimum of $0.77\,\mathrm{cm}^{-1}$ is achieved at $2000\,\mu$m (see Fig. 8, where the data for samples fabricated from high-purity raw materials are plotted). A comparison of paratellurite with other potential media for acousto-optics in the THz range (AlSb, GaAs, Ge, Si, and GaP crystals) revealed its advantage in design of AO devices [32]. The AO quality of paratellurite

turned out to be orders of magnitude higher. In this case, an absorption coefficient at the level of several cm^{-1} is not a critical value restricting the application of a material.

The optical characteristics of single crystals grown from different raw materials and procured from different manufacturers are compared in Fig. 9. The crystallographic orientation of samples corresponds to the (001) plane. In the UV and visible ranges, crystals grown from raw materials with an impurity concentration being three orders of magnitude higher (chemically clean raw materials with an impurity content reaching 0.5 wt.%) have close transmittance values. A similar pattern is observed for transmittance in other directions (corresponding to the (100) and (110) crystallographic planes; see Fig. 10). However, the transmittance value determined in this case for paratellurite grown from high-purity raw materials turned out to be 5 – 9% lower than the one corresponding to other samples.

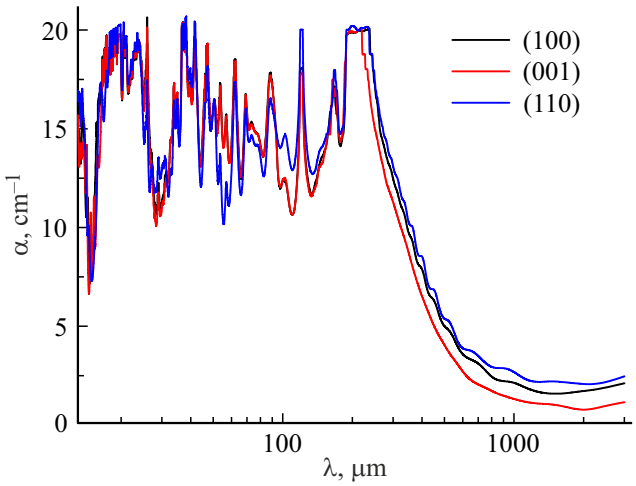

Figure 8. Terahertz absorption spectrum of paratellurite of different crystallographic orientations obtained from high-purity raw materials.

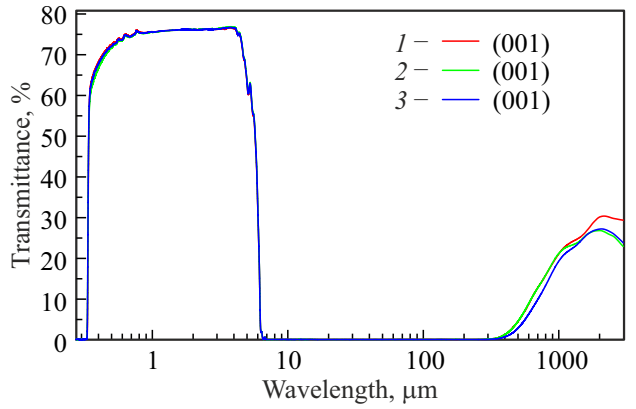

Figure 9. Transmittance spectrum of paratellurite obtained at TSU from high-purity (*1*) and chemically clean (*2*) raw materials and at the „Elent A“ enterprise (*3*) (plane (001)).

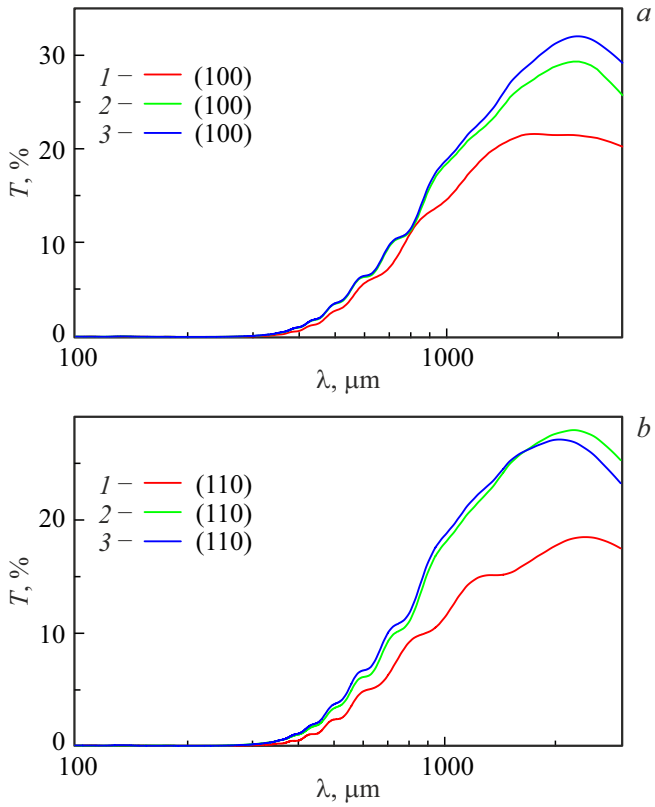

Figure 10. Transmittance spectrum of paratellurite obtained at TSU from high-purity (*1*) and chemically clean (*2*) raw materials and at the „Elent A“ enterprise (*3*). (*a*) Plane (100); (*b*) plane (110).

Conclusion

The optical transmittance and reflectance of paratellurite single crystals were studied within the 0.185 – 3000 μm spectral range for different crystallographic directions ([110], [100], and [001]). The influence of quality of raw materials of different purity and the specifics of fabrication procedures used by different manufacturers on the transmittance of samples was examined. It was demonstrated that the optical transmittance remains virtually unaffected by the purity of raw materials even when the impurity concentration decreases by three orders of magnitude.

It was established that the roughness parameters of different planes of paratellurite polished under the same conditions differ by a factor of 2 – 3. This may affect the absolute value of reflectance. The reflectance spectra featuring a series of minima and maxima within the 10 – 100 μm range were analyzed, and it was hypothesized that their emergence is related to the wave interference effect associated with the optical processing technology.

The transmittance value and the attenuation coefficient of paratellurite at a wavelength of 355 nm were measured: 64% and less than 0.092 cm^{-1}, respectively. This makes it suitable for construction of AO two-coordinate deflectors operating in the indicated range.

A reduction in the absorption coefficient in the region above $300-400\,\mu$m, which indicates the possibility of application of paratellurite in the THz wavelength range, was detected.

Funding

This study was carried out under state research assignment Nos. 75-03-2022-056 and 0817-2023-0006. Equipment provided by the Common Use Center of the Tver State University and Tydex LLC was used.

Conflict of interest

The authors declare that they have no conflict of interest.

References

[1] A.A. Blistanov, V.S. Bondarenko, N.V. Perelomova, F.N. Strizhevskaya, V.V. Chkalova, M.P. Shaskol'skaya. *Akusticheskie kristally. Spravochnik* (Nauka, M., 1982) (in Russian).
[2] J. Xu, R. Stroud. *Acousto-Optic Devices: Principles, Design and Applications* (John Wiley and Sons, NY., 1992).
[3] A.P. Goutzoulis, D.R. Pape. *Design and Fabrication of Acousto-Optic Devices* (Marcel Dekker, NY.,1994).
[4] V.Ya. Molchanov, Yu.I. Kitaev, A.I. Kolesnikov, V.N. Narver, A.Z. Rozenshtein, N.P. Solodovnikov, K.G. Shapovalenko. *Teoriya i praktika sovremennoi akustooptiki* (MISiS, M., 2015) (in Russian).
[5] L.N. Magdich, V.Ya. Molchanov. *Acoustooptic devices and their applications* (Gordon and Breach Science Pub., NY., 1989).
[6] A.A. Afonin, A.S. Guk, V.N. Nikitin, N.V. Nikitin, A.V. Shatskii, V.B. Chemodanov. *Navedenie lazernykh puchkov: Avtomaticheskie sistemy i ustroistva navedeniya.* 2nd ed. (URSS, M., 2023) (in Russian).
[7] V.Ya. Molchanov, S.I. Chizhikov, O.Yu. Makarov, N.P. Solodovnikov, V.N. Ginzburg, E.V. Katkin, E.A. Khazanov, V.V. Lozhkarev, I.V. Yakovlev. Acta Physica Polonica, **116** (3), 335 (2009). DOI: 10.12693/APhysPolA.116.355
[8] P.G. Kryukov. Quantum Electronics, **31** (2), 95 (2001). DOI: 10.1070/QE2001v031n02ABEH001906.
[9] O. Svelto. *Principles of Lasers* (Springer, 2007).
[10] A.S. Guk, Yu.V. Gulyaev, V.L. Evstigneev, M.A. Kazaryan, Yu.M. Mokrushin, M.A. Talalaev, O.V. Shakin. *Temperaturnye effekty v akustoopticheskikh deflektorakh na paratellurite* (Izd. Ross. Akad. Nauk, 2017) (in Russian).
[11] V.P. Zarubin, A.A. Karabutov, K.B. Yushkov, A.I. Chizhikov, O.Y. Makarov, V.Y. Molchanov, E.B. Cherepetskaya, S.A. Tretiakov, A.I. Kolesnikov. NDT & E International, **98** (2), 171 (2018). DOI: 10.1016/j.ndteint.2018.05.010
[12] S. Tretiakov, A. Kolesnikov, I. Kaplunov, R. Grechishkin, E. Shmeleva, K. Yushkov. Intern. J. Thermophysics, **37** (1), 1 (2016). DOI: 10.1007/s10765-015-2017-x
[13] S. Tretiakov, R. Grechishkin, A. Kolesnikov, I. Kaplunov, K. Yushkov, V. Molchanov, B.B.J. Linde. Acta Physica Polonica A, **127** (1), 72 (2015). DOI: 10.12693/APhysPolA.127.72
[14] V.I. Balakshii, V.N. Parygin, L.E. Chirkov. *Fizicheskie osnovy akustooptiki* (Radio i Svyaz', M., 1985) (in Russian).
[15] V.Ya. Molchanov, S.I. Shizhikov, O.Yu. Makarov. J. Phys.: Conf. Ser., **278**, 102 (2011). DOI: 10.1088/1742-6596/278/1/012016
[16] V.Ya. Molchanov, S.I. Chizhikov, O.Yu. Makarov, N.P. Solodovnikov, V.N. Ginzburg, E.V. Katin, E.A. Khazanov, V.V. Lozhkarev, I.V. Yakovlev. Appl. Optics, **48** (7), 118 (2009). DOI: 10.12693/APhysPolA.116.355
[17] V.Ya. Molchanov, S.I. Chizhikov, K.B. Yushkov. Quantum Electron., **41** (8), 675 (2011). DOI: 10.1070/QE2011v041n08ABEH014676.
[18] Yu.V. Egorov, K.P. Naumov, V.N. Ushakov. *Akustoopticheskie protsessy* (Radio i Svyaz', M., 1991) (in Russian).
[19] S.V. Kulakov. *Akustoopticheskie ustroistva spektral'nogo i korrelyatsionnogo analiza signalov* (Nauka, L., 1978) (in Russian).
[20] J.N. Lee, A. Vanderugt. Proc. IEEE, **77** (10), 1528 (1989).
[21] E.Yu. Vorontsova, R.M. Grechishkin, I.A. Kaplunov, A.I. Kolesnikov, I.V. Talyzin, S.A. Tret'yakov, V.Ya. Molchanov. Opt. Spectrosc., **104** (6), 886 (2008).
[22] G. Boivin, P. Bélanger, R.J. Zednik. Crystals, **10**, 939 (2020). DOI: 10.3390/cryst10100939
[23] C. Arnaboldi, C. Brofferio, A. Bryant, C. Bucci, L. Canonica, S. Capelli, M. Carrettoni, M. Clemenza, I. Dafinei, S. Di Domizio, F. Ferroni, E. Fiorini, Z. Ge, A. Giachero, L. Gironi, A. Giuliani, P. Gorla, E. Guardincerri, R. Kadel, K. Kazkaz, L. Kogler, Y. Kolomensky, J. Larsen, M. Laubenstein, Y. Li, C. Maiano, M. Martinez, R. Maruyama, S. Nisi, C. Nones, E.B. Norman, A. Nucciotti, F. Orio, L. Pattavina, M. Pavan, G. Pessina, S. Pirro, E. Previtali, C. Rusconi, N.D. Scielzo, M. Sisti, A.R. Smith, W. Tian, M. Vignati, H. Wang, Y. Zhu. J. Crystal Growth, **312** (20), 2999 (2010). DOI: 10.1016/j.jcrysgro.2010.06.034
[24] F. Bellinia, M. Biassonic, C. Buccie, N. Casalia, I. Dafinei, Z. Ge, P. Gorla, F. Ferroni, F. Orio, C. Tomei, M. Vignati, Y. Zhu. J. Instrumentation, **5** (12), 12005 (2010). DOI: 10.1088/1748-0221/5/12/P12005
[25] F. Bellini, L. Cardani, N. Casali, I. Dafinei, M. Marafini, S. Morganti, F. Orio, D. Pinci, G. Piperno, D. Santone, C. Tomei, M. Vignati. J. Instrumentation, **9** (10), 10014 (2014). DOI: 10.1088/1748-0221/9/10/P10014
[26] L. Cardani, L. Gironi, J.W. Beeman, I. Dafinei, Z. Ge, G. Pessina, S. Pirro, Y. Zhu. J. Instrumentation, **7** (01), 01020 (2012). DOI: 10.1088/1748-0221/7/01/P01020
[27] V.Yu. Zheleznov, T.V. Malinsky, V.E. Rogalin, Yu.V. Khomich, V.A. Yamshchikov, I.A. Kaplunov, A.I. Ivanova. Izvestiya Vysshikh Uchebnykh Zavedenii. Materialy Elektronnoi Tekhniki = Materials of Electronics Engineering, **26** (2), 89 (2023) (in Russ.). DOI: 10.17073/1609-3577-2023-2-89-100. EDN: KWMYIJ.
[28] Gennadiy Komandin, Vadim Nozdrin, Sergey Chuchupal, Vladimir Lomonov, Yurii Pisarevskii, Oleg Porodinkov, Igor Spektor. J. Phys. D: Appl. Phys., **53**, 495102 (2020). DOI: 10.1088/1361-6463/abafdc
[29] M. Sotome, N. Kida, R. Takeda, H. Okamoto. Phys. Rev. A, **90**, 033842 (2014). DOI: 10.1103/PhysRevA.90.033842
[30] M. Unferdorben, A. Buzády, J. Hebling, K. Kiss, I. Hajdara, L. Kovács, Á. Péter, L. Pálfalvi. J. Infrared Milli Terahz Waves, **37**, 703 (2016). DOI: 10.1007/s10762-016-0261-1
[31] D.L. Porokhovnichenko, V.B. Voloshinov, E.A. Dyakonov, G.A. Komandin, I.E. Spektor, V.D. Travkin. Phys. Wave Phenom., **25** (2), 114 (2017). DOI: 10.3103/S1541308X17020066
[32] P.A. Nikitin. Svetotekhnika, **5**, 52 (2022) (in Russian).

[33] J. Janszky, A. Peter, A. Mecseki. Kristallografiya, **27** (1), 152 (1982) (in Russian).
[34] I.A. Kaplunov, A .I. Kolesnikov, I.V. Talyzin, S.L. Shaĭovich. J. Opt. Technol., **72** (3), 271 (2005). DOI: 10.1364/JOT.72.000271.
[35] I.A. Kaplunov, A.I. Kolesnikov, K.P. Skokov, R.M. Grechishkin, L.V. Sedova, S.A. Tret'yakov. J. Opt. Technol., **72** (7), 572 (2005). DOI: 10.1364/JOT.72.000572.
[36] A.V. Vinogradov, V.A. Lomonov, Yu.A. Pershin, N.L. Sizova. Crystallography Reports, **47** (6), 1036 (2002). DOI: 10.1134/1.1523523.
[37] A.I. Kolesnikov, I.A. Kaplunov, I.A. Terent'ev. Crystallography Reports, **49** (2), 180 (2004).
[38] A.E. Kokh, V.S. Shevchenko, V.A. Vlezko, K.A. Kokh. J. Crystal. Growth, **384**, 1 (2013). DOI: 10.1016/J.JCRYSGRO.2013.08.027
[39] P. Veber, J. Mangin, P. Strimer, P. Delarue, C. Josse, L. Saviot. J. Crystal Growth, **270** (1), 77 (2004). DOI: 10.1016/j.jcrysgro.2004.06.029
[40] A.I. Kolesnikov, A.V. Shelopaev, I.A. Kaplunov, I.V. Talyzin, E.Yu. Vorontsova. Izv. Vyssh. Uchebn. Zaved., Mater. Elektron. Tekh., **4**, 27 (2009) (in Russian).
[41] A.I. Kolesnikov, I.A. Kaplunov, S.E. Ilyashenko, V.Ya. Molchanov, R.M. Grechishkin, M.A. Arkhipova, S.A. Tretyakov. Crystallography Reports, **57**, 909 (2012). DOI: 10.1134/S1063774512070115
[42] S. Kumaragurubaran, D. Krishnamurthy, C. Subramanian, P. Ramasamy. J. Crystal Growth, **197** (1–2), 210 (1999). DOI: 10.1016/S0022-0248(98)00788-X
[43] S. Kumaragurubaran, D. Krishnamurthy, C. Subramanian, P. Ramasamy. J. Crystal Growth, **211** (1–4), 276 (2000). DOI: 10.1016/S0022-0248(99)00834-9
[44] Ya. Chu, Ya. Li, Z. Ge, G. Wu, H. Wang. J. Crystal Growth, **295** (2), 158 (2006). DOI: 10.1016/j.jcrysgro.2006.08.009
[45] J. Liebertz. Kristall und Technik, **4** (2), 221 (1969). DOI: 10.1002/crat.19690040205
[46] N. Uchida. Phys. Rev. B, **4** (10), 3746 (1971).
[47] P.A. Thomas. J. Phys. C: Solid State Phys., **21** (25), 4611 (1988). DOI: 10.1088/0022-3719/21/25/009
[48] D.M. Korn, A.S. Pine, G. Dresselhaus, T.B. Reed. Phys. Rev. B, **8** (2), 768 (1973). DOI: 10.1103/PhysRevB.8.768
[49] G. Komandin, V. Nozdrin, S. Chuchupal, V. Lomonov, Yu. Pisarevskii, O. Porodinkov, I. Spektor. J. Phys. D: Appl. Phys., **53**, 495102 (2020). DOI: 10.1088/1361-6463/abafdc
[50] M.A. Okatov. *Spravochnik tekhnologa-optika* (Politekhnika, S-Pb., 2004) (in Russian).
[51] M.V. Kurik. J. Appl. Spectrosc., **4** (3), 199 (1966). DOI: 10.1007/BF00612152.
[52] I.A. Kaplunov, A.I. Kolesnikov, I.V. Talyzin, L.V. Sedova, S.L. Shaĭovich. J. Opt. Technol., **72** (7), 564 (2005). DOI: 10.1364/JOT.72.000564.
[53] Refractive Index. INFO [electronic source]. Available at: https://refractiveindex.info
[54] I.A. Kaplunov, G.I. Kropotov, V.E. Rogalin, A.A. Shahmin. Opt. Spectrosc., **128** (10), 1583 (2020). DOI: 10.1134/S0030400X20100136.

Translated by D.Safin